

YfeX – A New Platform for Carbene Transferase Development with High Intrinsic Reactivity

Victor Sosa Alfaro,^[a] Sodiq O. Waheed,^[b] Hannah Palomino,^[a] Anja Knorrscheidt,^[c] Martin Weissenborn,^[c] Christo Z. Christov,^{*,[b]} and Nicolai Lehnert^{*,[a]}

Abstract: Carbene transfer biocatalysis has evolved from basic science to an area with vast potential for the development of new industrial processes. In this study, we show that YfeX, naturally a peroxidase, has great potential for the development of new carbene transferases, due to its high intrinsic reactivity, especially for the N–H insertion reaction of aromatic and aliphatic primary and secondary amines. YfeX shows high stability against organic solvents (methanol and DMSO), greatly improving turnover of hydrophobic substrates. Interestingly, in styrene cyclopropanation, WT YfeX

naturally shows high enantioselectivity, generating the *trans* product with 87% selectivity for the (R,R) enantiomer. WT YfeX also catalyzes the Si–H insertion efficiently. Steric effects in the active site were further explored using the R232A variant. Quantum Mechanics/Molecular Mechanics (QM/MM) calculations reveal details on the mechanism of Si–H insertion. YfeX, and potentially other peroxidases, are exciting new targets for the development of improved carbene transferases.

Introduction

Carbene transfer reactions are an important route in organic synthesis since they generate hard to synthesize carbon-carbon and carbon-heteroatom bonds, and, importantly, these methods can be used in late-stage functionalization of larger molecules, especially drug precursors.^[1–8] Different methods for carbene transfer reactions have previously been developed utilizing transition-metal complexes of Rh(II), Ir(III), Au(I) and Pd(II) that catalyze the decomposition of diazo reagents to form an electrophilic metal-carbene unit, which is subsequently attacked by a nucleophilic reagent such as an olefin (for cyclopropanation) or an amine (for N–H insertion), etc.^[8–11]

These methods have a negative impact on the environment once they are scaled up in industry due to the need for expensive rare metals, and the usage of organic solvents during catalysis, which generates large amounts of waste.^[1,12–16] The implementation of biocatalysis for C–H functionalization is an attractive avenue due to the ability of metalloenzymes to operate under environmentally friendly conditions, at high rates and with high stereo- and enantioselectivity.^[17,18] These biological catalysts lead to a significant reduction in waste and cost in industrial-scale synthesis compared to stoichiometric syntheses and other catalytic processes.^[19,20] In recent years, multiple groups have sought to modify heme proteins (containing Fe porphyrin cofactors) to produce new types of stereoselective and water-soluble carbene transferases.^[21–26] These enzymatic reactions take place under mild conditions and do not require toxic solvents with negative effects on the environment.^[19,24,27,28]

As pointed out by Arnold and coworkers, in the choice and subsequent development of a proper biocatalyst, *wild-type (WT) enzymes with high intrinsic reactivity should be used as a starting point for further catalyst optimization*. The latter includes the following engineering of biocatalysts to achieve broad substrate scope, high catalytic efficiency, and good site- and stereoselectivity.^[29] Hence, there is a need to identify WT enzymes with high intrinsic reactivity, to broaden the substrate and reaction scope of biocatalysts. Protein engineering tools such as rational design,^[30] directed evolution,^[6] and de novo design^[26,31] aid to improve/tune the enzymatic activity for a desired transformation and enhance abiological reactivity. These methods target specific amino acids within the active site and beyond to help increase desired traits. Initial efforts in the field were directed towards Cytochrome (Cyt.) P450s,^[32] a superfamily of heme-containing monooxygenases, and it has been shown by Arnold and coworkers that they can be

[a] V. Sosa Alfaro, H. Palomino, Prof. Dr. N. Lehnert
Department of Chemistry and Department of Biophysics
University of Michigan
Ann Arbor, Michigan 48109–1055 (United States)
E-mail: lehnertn@umich.edu
Homepage: <http://www.umich.edu/~lehnert/>

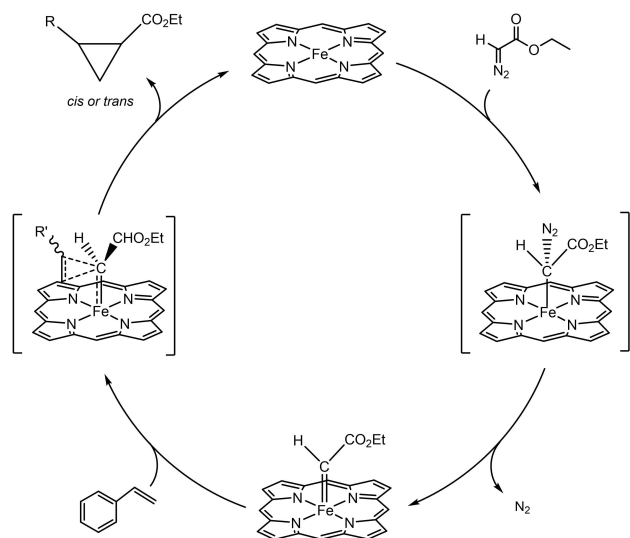
[b] S. O. Waheed, Prof. Dr. C. Z. Christov
Department of Chemistry
Michigan Technological University
Houghton, Michigan 49931 (United States)
E-mail: christov@mtu.edu
Homepage: <https://chem.sites.mtu.edu/christov/>

[c] A. Knorrscheidt, Prof. Dr. M. Weissenborn
Institute of Chemistry
Martin-Luther-University Halle-Wittenberg
Kurt-Mothes-Str. 2, 06120 Halle (Germany)

Supporting information for this article is available on the WWW under <https://doi.org/10.1002/chem.202201474>

© 2022 The Authors. Chemistry - A European Journal published by Wiley-VCH GmbH. This is an open access article under the terms of the Creative Commons Attribution Non-Commercial NoDerivs License, which permits use and distribution in any medium, provided the original work is properly cited, the use is non-commercial and no modifications or adaptations are made.

engineered to do abiological reactions with high activity.^[2–6] In this way, hemoprotein engineering has been used to expand novel enzyme activity not known in the biological world, such as a recent report of biocatalytic carbon-silicon bond formation.^[29] Besides Cyt. P450s, another heme protein that has extensively been used for biocatalyst development is myoglobin (Mb).^[33–36] In this case, however, the choice of Mb was largely guided by the stability and ease of access to this protein. As we show in this paper, the use of an enzyme with a well-shielded active site within the protein scaffold (in contrast to Mb) may ultimately be beneficial for biocatalyst development.



Scheme 1. Cyclopropanation mechanism of heme enzymes via carbene insertion.^[7,81]

Carbene transferases are of particular interest in the quickly developing field of organometallic biocatalysis. Utilizing nature as an inspiration, our laboratory and others have developed carbene transfer biocatalysts based on heme-containing enzymes such as Mb.^[33–45] Scheme 1 shows the general mechanism of carbene transfer reactions, starting from a diazo compound, here ethyl diazoacetate (EDA), which reacts with the heme, generating a metal-carbenoid intermediate while releasing dinitrogen, shown at the bottom of the scheme. Next, substrate binds within the heme pocket, in this case styrene, and reacts with the carbenoid intermediate generating a cyclopropane ethyl acetate product and regenerating the heme in its active state. Further engineering strategies can then be used to facilitate carbene insertion reactions, optimize selectivity, and broaden the substrate scope of the reactions to generate high value products.

Recently, our focus has shifted to the use of YfeX, a novel heme protein found to have native peroxidase-like activity in *E. coli*.^[46–48] Peroxidases have generally not been investigated much for biocatalytic applications in carbene transfer, in contrast to Cyt P450s and Mb. As we show in this work, this neglect is unjustified, as peroxidases are great platforms for biocatalyst development. Initial work by some of us (Weissenborn and coworkers) showed that WT YfeX can catalyze carbonyl olefination reactions with turnover numbers TON up to 16 under optimized conditions.^[49] Unlike Mb, which has an exposed heme in a cleft-like heme pocket with a distal histidine, YfeX contains a buried heme in a large active site that contains charged amino acids in the second coordination sphere (SCS), including a key distal arginine residue (Figure 1). The active site is connected to the protein surface via a tunnel, which, in the native peroxidase reaction of YfeX, is proposed to guide

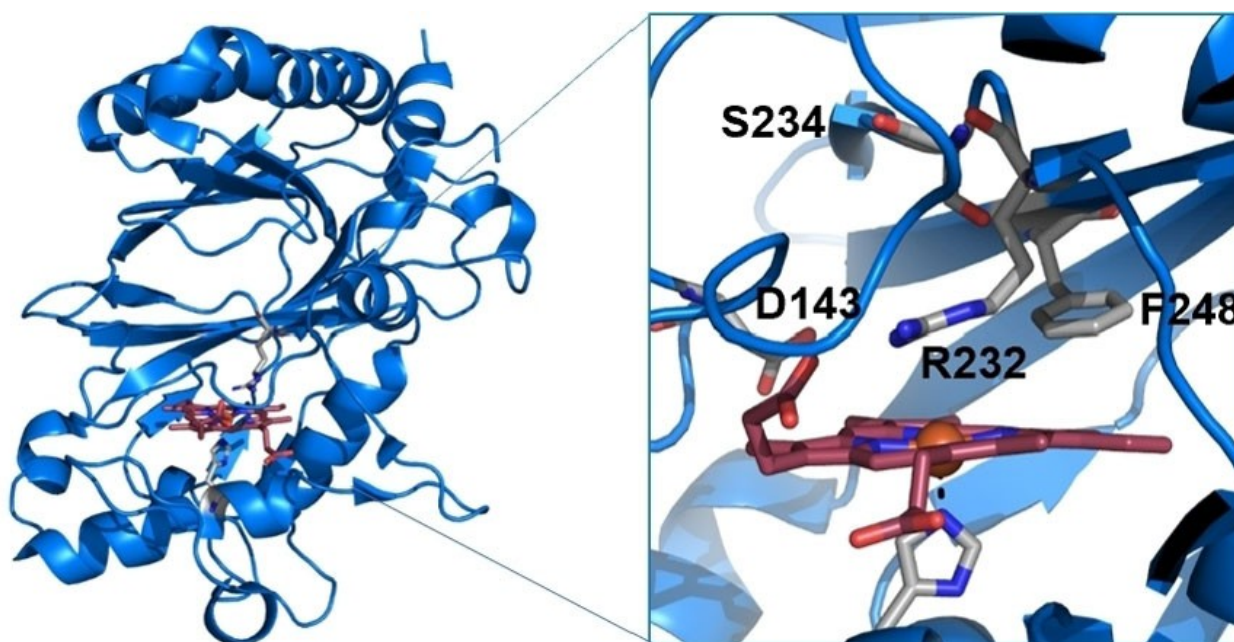


Figure 1. Pymol representation of the crystal structure of YfeX (left), and of the active site with important SCS amino acids highlighted (PDB code: 2IIZ).

hydrogen peroxide to the active site.^[47] This tunnel is important, as the substrates for abiological carbene transfer catalysis with YfeX also must enter the active site via this tunnel. These distinct features of Mb versus YfeX contribute to the different reactivity profiles of these proteins, as discussed in detail in this paper.

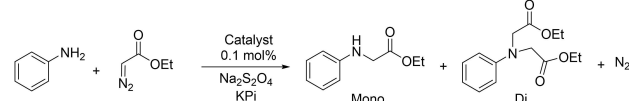
In this work, we investigated the basic catalytic abilities of YfeX as a carbene transferase, using olefins, primary and secondary aromatic and aliphatic amines, and silanes as substrates. Here, we focused on the investigation of substrate scope, reaction kinetics, and the pH dependence of the observed reactivity. To explore the steric effects of the SCS in the active site on catalysis, we also studied the catalytic activity of the YfeX variant R232A and compared it to WT enzyme. Moreover, we modified the active site by incorporating Ru-mesoporphyrin IX (RuMpIX) and Co-protoporphyrin IX (CoPpIX) into apo YfeX to determine whether catalytic activity can be further improved by use of unnatural cofactors. This work establishes WT YfeX as an excellent platform for biocatalyst development compared to WT Mb, with a high intrinsic reactivity, especially for N–H and Si–H insertion reactions. Furthermore, utilizing both molecular dynamics (MD) simulations and combined Quantum Mechanics/Molecular Mechanics (QM/MM) calculations, we analyzed the atomistic and electronic structure factors that contribute to the stability of the metal-carbenoid complex and then explored the reaction mechanism of Si–H insertion by YfeX. The study offers general insight into the role of the SCS in YfeX for carbene transfer reactions, and in this way, identifies targets for future mutagenesis studies to further improve catalysis with YfeX, especially selectivity. These studies are ongoing.

Results

Wild-type YfeX Carbene Insertion Reactivity

Initial work focused on the carbene transfer reactivity of wild-type (WT) YfeX using two different carbene transfer reactions: N–H insertion and cyclopropanation. As shown in Table 1, the N–H insertion activity of YfeX with aniline as the substrate is higher (72% yield) compared to [Fe^{II}PpIX] (27% yield) and sperm whale (SW) WT Mb (21% yield).^[50] We achieved the highest Turnover Number (TON) of 6274 for this reaction using 0.001% catalyst loading over 20 h. Additionally, at higher YfeX loading aniline is able to produce the mono- (usual product) and di-insertion product (diethyl 2,2-(phenylimino) diacetate) with EDA (see header of Table 1). At 0.1% catalyst loading, 30% of the disubstitution product is obtained, but as the catalyst loading is reduced (or, in other words, the excess of aniline is increased), the disubstitution reaction is suppressed. In fact, at 0.01% catalyst loading, the di-insertion product only contributes 1% to the total yield. This result directly shows that after the first N–H insertion, the monosubstituted product is released from the YfeX active site, and then enters the active site again to generate the disubstituted product. If the monosubstituted product would remain in the YfeX active site and react again to

Table 1. Results for the N–H insertion reaction of aniline with WT YfeX.



Catalyst	Total Yield ^[a] (%)	TON	Mono:Di
[Fe ^{II} PpIX]	27	271 ± 38	
SW Mb ^[b]	21	210	
YfeX (0.1 mol%)	72	724 ± 32	70:30
YfeX (0.01 mol%)	27	2658 ± 274	99:1
YfeX (0.001 mol%)	3	3026 ± 573	100:0
YfeX (0.001 mol%) ^[c]	6	6274 ± 226	100:0
YfeX R232A (0.1 mol%)	76	756 ± 64	72:28

[a] Reaction conditions: 20–0.2 μM YfeX (0.1–0.001 mol%), 20 mM aniline, 40 mM EDA, 10 mM dithionite, 1 h reaction time in 50 mM phosphate buffer (pH 7.4). Yields are based on GC/MS analysis. [b] Based on studies by Sreenilayam et al.^[50] The yield was determined after 16 h reaction time. [c] The yield was determined after 20 h reaction time.

yield the disubstituted product, the yield of the disubstituted product would **not** decrease substantially upon an increase in substrate concentration (= decrease in catalyst loading). On the other hand, if the monosubstituted product is released from the active site, then a large excess of aniline would statistically decrease the likelihood of monosubstituted product to become disubstituted, and this is what we observe experimentally. In this way, the ratio of mono- to di-insertion product can be directly controlled in YfeX catalysis.

Recently, Fasan and coworkers have shown that WT Mb and variants can also generate the di-insertion product, but only with benzylamine as the substrate (at 1:13 mono:di product ratio). They further engineered Mb to have higher reactivity and, by lowering the catalyst loading, the mono-insertion product can again be produced as the main product.^[51] It was further shown that when more sterically demanding amino acids were introduced into the Mb active site, for example via the double mutant Mb(H64G, V68A), the amount of disubstituted benzylamine product was not affected. The disubstitution in this case could only be suppressed by reducing catalyst loading.^[51] Similarly, our results show that YfeX's relative larger active site can also promote the disubstitution of aniline, with increased mono-substitution when catalyst loading is reduced. Here, the mono- to disubstitution ratio can further be controlled by modifying the substrate loading. At low EDA concentration (1:4 EDA:aniline) 99% mono-substitution is observed. Conversely, at high EDA concentration (4:1 EDA:aniline), 51% disubstituted product is obtained.

Time course kinetic measurements were further conducted for the N–H insertion reaction of aniline by monitoring the yield of monosubstituted product via GC/MS. It was found that YfeX has a $k_{\text{obs}} = 0.210 \text{ min}^{-1}$, as shown in Figure 2.

In contrast to the outstanding N–H insertion activity of YfeX, the cyclopropanation reaction with this protein generates a 27% yield with a TON of 268, which is comparable to that of WT Mb (36% yield, with a TON of 180).^[23] Further analysis of the styrene cyclopropane product shows a *cis* to *trans* ratio of the product of 11 to 89 (see Table 2), again comparable to WT Mb

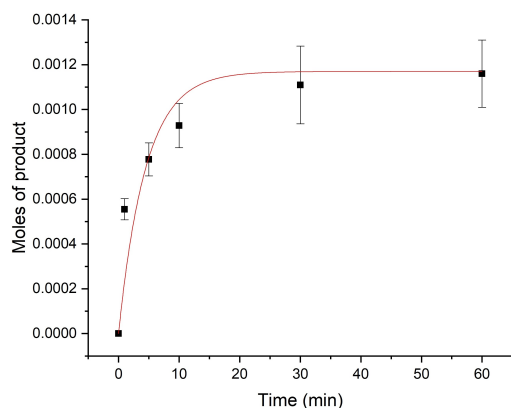


Figure 2. Time course of the N–H insertion reaction of aniline catalyzed by YfeX. The catalyst was prepared at 20 μM concentration and reduced with 500 equivalents of $\text{Na}_2\text{S}_2\text{O}_4$ before addition of 1000 equivalents of aniline and 2000 equivalents of EDA to a final volume of 500 μL . The organic products were extracted with 3 mL of ethyl acetate after the following time points: 2, 5, 10, 30, and 60 minutes. Finally, the product was quantified by GC/MS. Exponential fit of the data gives a $k_{\text{obs}} = 0.210 \text{ min}^{-1}$.

Table 2. Results for the cyclopropanation reaction of styrene with WT YfeX.

Catalyst	Total Yield ^[a] (%)	TON	Cis:Trans ^[b]	(R,R) Trans ^[b]
[Fe ^{II} PpIX]	16	158 \pm 64	13:87	
WT Mb	36 ^[c]	180 \pm 28	7:93	47%
YfeX	27	268 \pm 72	11:89	87%
YfeX ^[d]	47	474 \pm 15	9:91	87%
YfeX ^[e]	59	593 \pm 81	9:91	88%

[a] Reaction conditions: 20 μM YfeX (0.1 mol%), 20 mM styrene, 40 mM EDA, 10 mM dithionite, 1 h reaction time in 50 mM phosphate buffer (pH 7.4). [b] Values determined by GC/MS or supercritical fluid chromatography. [c] Based on studies by Bajaj et al.^[23] Reaction conditions: 20 μM Mb (0.1 mol%), 10 mM styrene, 20 mM EDA, 10 mM dithionite, 16 h reaction time. [d] Reaction performed in 30% methanol. [e] Reaction performed in 30% DMSO.

(7:93) and [Fe^{II}PpIX] (13:87), indicating that the protein matrix of YfeX is not interfering with the natural *cis:trans* selectivity of iron-porphyrins. In addition, YfeX forms the *trans* product with 87% selectivity for the (R,R) enantiomer, which is different from WT Mb, which produces 47% (R,R) enantiomer.^[23] This difference in enantioselectivity is surprising, and indicates that either the orientation of the carbene ligand in the YfeX active site is more restricted, or that the styrene substrate predominantly enters the active site of YfeX in a predefined orientation. The fact that the N–H insertion reactivity of YfeX is much more robust than its cyclopropanation reactivity further indicates that the relatively low yield of cyclopropanes is not related to problems with the generation of the carbene intermediate or its reactivity, but rather with substrate (styrene) access to the YfeX active site via the enzyme's substrate channel.

The stability of YfeX was further investigated under catalytic conditions by UV-vis spectroscopy. Our results show that WT

YfeX is as stable as WT Mb.^[35] after addition of EDA to a reduced sample of YfeX, the Soret band of the heme shifts to 430 nm (similar to what is seen with WT Mb and Rma TDE),^[35,52] and this carbenoid species is stable for 60+ minutes (Figure S1). The small decrease of the Soret band at 430 nm after 20 minutes is indicative of a small amount of the YfeX decomposing (Figure S1). One of the important steps in the cyclopropanation reaction is substrate access to the active site. Styrene, a non-polar substrate with low water solubility, requires hydrophobic interactions to go into and stably bind in the active site of a protein. However, the active site of YfeX, shown in Figure 1, is overall hydrophilic due to three prominent amino acids, D143, S234, and R232 (discussed below). The low solubility of styrene in buffer combined with the high polarity of the substrate channel and active site of YfeX could be responsible for the low cyclopropanation yields. Kinetic measurements were conducted by monitoring the styrene cyclopropanation yields via GC/MS over time. It was found that YfeX has a $k_{\text{obs}} = 0.096 \text{ min}^{-1}$ for cyclopropanation (see Figure 3), which is distinctively smaller than the rate constant obtained for the N–H insertion reaction, in agreement with the higher yield for the latter reaction in 1 h.

Substrate Scope of the Carbene Transfer Reactions

Since YfeX is an outstanding catalyst for the N–H insertion reaction, we further investigated its substrate scope. The N–H insertion reaction of secondary amines was investigated using *N*-methyl aniline as a substrate, giving a 62% yield with a TON of 620 (see Table 3). This result further confirms that di-insertion of aniline with EDA is due to the inherent reactivity of WT YfeX towards primary and secondary N–H bonds. Further substrate scope studies for the N–H insertion reaction used anilines with electron-withdrawing (4-bromoaniline, 4-trifluoromethylaniline) and electron-donating (4-methylthioaniline, 4-methoxy-6-methylaniline, *p*-toluidine) substituents. The electron-rich substrates

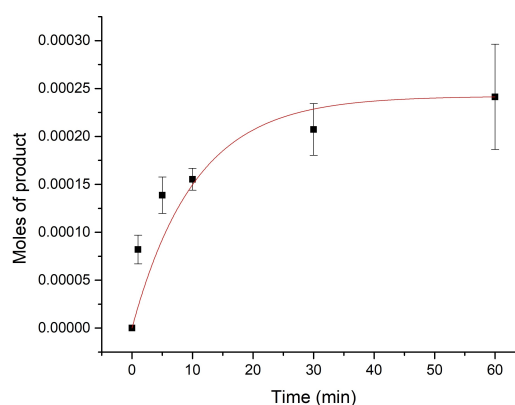
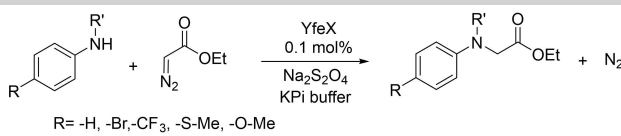


Figure 3. Time course of the cyclopropanation reaction of styrene catalyzed by YfeX. The catalyst was prepared at 20 μM concentration and reduced with 500 equivalents of $\text{Na}_2\text{S}_2\text{O}_4$ before addition of 1000 equivalents of styrene and 2000 equivalents of EDA at final volume of 500 μL . The organic products were extracted with 3 mL of ethyl acetate after the following time points: 2, 5, 10, 30, and 60 minutes. Finally, the product was quantified by GC/MS. Exponential fit of the data gives a $k_{\text{obs}} = 0.096 \text{ min}^{-1}$.

Table 3. Results for the N–H insertion reaction of aniline derivatives with WT YfeX.


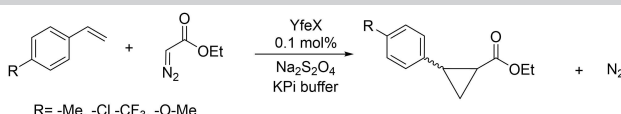
R = -H, -Br, -CF₃, -S-Me, -O-Me
R' = -H, -Me

Substrate	Total Yield ^[a] (%)	TON	Mono:Di
N-methyl aniline	62	623 ± 36	100:0
4-bromoaniline	40	404 ± 62	100:0
4-trifluoromethylaniline	51	510 ± 25	100:0
4-methylthiolaniline	57	568 ± 48	100:0
4-methoxy-6-methyl aniline	52	515 ± 49	43:57
p-toluidine	57	571 ± 19	49:50
o-toluidine	28	279 ± 30	64:36
m-toluidine	37	374 ± 19	43:57
benzylamine ^[b]	56	558 ± 28	0:100
4-nitroaniline ^[b]	25	248 ± 23	100:0

[a] Reaction conditions: 20 μM YfeX (0.1 mol%), 20 mM aniline derivative, 40 mM EDA, 10 mM dithionite, 1 h reaction time in 50 mM phosphate buffer (pH 7.4). Yields are based on GC/MS analysis. [b] Reactions were run in 30% methanol.

give 52–57% yield, indicating a preference for electron-rich substrates, whereas the electron-poor substrates give 40–51% yield. Here, the electron-withdrawing –Br and –CF₃ groups are expected to decrease the nucleophilicity of the aniline and thus exhibit less reactivity with the electrophilic Fe-carbene intermediate. Furthermore, the steric effects within the active site pocket were analyzed utilizing *ortho*-, *meta*- and *para*-toluidine as the substrates. As the methyl group moves closer to the reactive amine group, from *para* to *meta* to *ortho* substitution, the N–H insertion yields decrease accordingly, from 57% to 37% to 23% (see Table 3).

The substrate scope for the cyclopropanation reaction was also investigated using WT YfeX. Various *para*-substituted styrene derivatives were examined for cyclopropanation activity, with the functional groups analogous to the aniline derivatives discussed above (see Table 4). 4-methylstyrene shows the highest yield with 48% compared to styrene and other derivatives. Vinylanisole, 4-chlorostyrene, and 4-trifluoromethylstyrene show a moderate conversion to the cyclopropane products with similar yields (30%, 23% and 29%,

Table 4. Results for the cyclopropanation reaction of styrene derivatives with WT YfeX.


R = -Me, -Cl, -CF₃, -O-Me

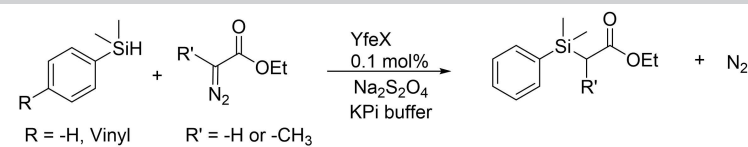
Substrate	Total Yield ^[a] (%)	TON	Cis:Trans
4-methylstyrene	48	484 ± 30	23:77
vinylanisole	30	297 ± 84	14:86
4-chlorostyrene	23	230 ± 33	13:87
4-trifluoromethylstyrene	29	293 ± 30	10:90

[a] Reaction conditions: 20 μM YfeX (0.1 mol%), 20 mM styrene derivative, 40 mM EDA, 10 mM dithionite, 1 h reaction time in 50 mM phosphate buffer (pH 7.4). Yields are based on GC/MS analysis.

respectively). Lower yields are expected for the substrates with the electron-withdrawing –Cl and –CF₃ groups, but not for vinylanisole with an electron-donating –OMe group. In the latter case, the lower yield might therefore be due to steric reasons. All of the substrates exhibit similar diastereoselectivity, yielding 80–90% of the *trans* isomer.

As discussed above, the N–H insertion with YfeX is greatly favored over the cyclopropanation reaction, which could be caused by the low solubility of styrene in the reaction medium. We sought to probe this hypothesis by improving substrate solubility, which can be accomplished by increasing the amount of the methanol co-solvent in the reaction mixtures (see Table S1). As the methanol concentration is increased to 10%, the yields for both aniline and styrene reactions remain unchanged. At a 30% methanol co-solvent concentration, the yield for the aniline-based product remains similar, but, importantly, a doubling of the yield for the styrene substrate is observed (47% yield). At 50% methanol co-solvent concentration, a decrease in product yield is observed in both reactions. Further characterization via circular dichroism spectroscopy showed that at 50% methanol co-solvent concentration, YfeX begins to unfold or aggregate, which is likely the reason for the decreased yields under these conditions (see Figure S8). We further show that 30% DMSO as a co-solvent further improves the cyclopropanation yield, with an increase to 59% (see Tables 2 and S1). Furthermore, two additional substrates with very low aqueous solubility were screened, 4-nitroaniline (25% yield) and benzylamine (double insertion, 56% yield) using 30% MeOH co-solvent (see Table 3). Overall, our results show that as the concentration of the methanol co-solvent increases, the solubility of styrene and other hydrophobic substrates increases accordingly, leading to greatly enhanced product yields. The optimal methanol concentration is ~30%.

Furthermore, utilizing dimethylphenylsilane as a substrate, we explored whether YfeX is able to catalyze the carbene insertion into silicon-hydrogen (Si–H) bonds. This reaction has so far only been observed in few examples. This includes WT Mb (turnover number (TON)=175 after 12 h using 0.2 mol% catalyst loading), horseradish peroxidase (HRP; TON=5 after 12 h at 0.2 mol% catalyst loading), WT *Rhodothermus marinus* Cyt. c (*Rma* Cyt. c; total turnover number (TTN)=44 ± 27) and others.^[29,53] Arnold and coworkers used directed evolution to further optimize *Rma* Cyt. c for this reaction, resulting in a triple mutant (V75T, M100D, M103E) that catalyzes Si–H insertion with TTN=1518 ± 51 with a diazoacetate.^[29] Excitingly, WT YfeX is able to catalyze the carbene transfer to dimethylphenylsilane, generating ethyl[dimethyl(phenyl)silyl] acetate in 11% yield with a TON of 108 at 0.1 mole percent of catalyst after just one hour (see Table 5), without any optimization. This finding emphasizes the potential of YfeX for further development into a highly versatile carbene transferase. Recently, the Arnold and Houk groups used conformational dynamics and mutagenesis experiments to further optimize catalysis with *Rma* Cyt. c. Based on their computational predictions, they were able to control the chemoselectivity of *Rma* Cyt. c for either N–H or Si–H insertion.^[54]

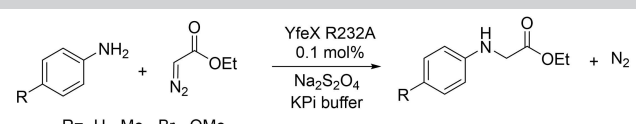
Table 5. Catalytic activity of YfeX for the Si–H insertion reaction.


Substrate	Catalyst	Total Yield (%)	Turnover	Ref.
dimethylphenylsilane	YfeX ^[a]	11	108 ± 33 ^[TON]	This work
dimethylphenylsilane	Rma Cyt. C ^[b]	–	44 ± 27 ^[TTN]	[29]
dimethylphenylsilane	Mb ^[c]	35	175 ^[TON]	[53]
4-(dimethylsilyl) styrene	HRP ^[c]	1	5 ^[TON]	[53]

[a] Reaction conditions: 20 μM YfeX (0.1 mol%), 20 mM dimethylphenylsilane, 40 mM EDA, 10 mM dithionite, 1 h reaction time. Yields are based on GC/MS analysis. [b] Yields based on 0.1 mol% catalyst loading for 1.5 h with Me-EDA. [c] Yields based on 0.2 mol% catalyst loading for 12 h with EDA.

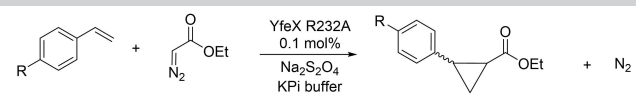
YfeX R232A Mutant

To begin analyzing the role of the second coordination sphere (SCS) within the YfeX active site for carbene transfer reactivity, the YfeX variant R232A was investigated, where the R232 residue that sits right above the heme is replaced with Ala. This choice was inspired by work on Mb, where removal of the distal His has a notable effect on catalysis.^[7,35] The N–H insertion with aniline and aniline derivatives for YfeX R232A shows interesting

Table 6. Results for the N–H insertion reaction of aniline with YfeX R232A.


Substrate	Total Yield ^[a] (%)	TON	Mono:Di
aniline	75	756 ± 64	83:17
<i>p</i> -toluidine	40	408 ± 4	67:33
<i>o</i> -toluidine	50	502 ± 8	80:20
<i>m</i> -toluidine	51	512 ± 96	54:46
4-bromoaniline	43	434 ± 78	87:13
<i>p</i> -anisidine	54	544 ± 23	56:44
4-trifluoromethylaniline	51	505 ± 67	83:17

[a] Reaction conditions: 20 μM YfeX R232A (0.1 mol%), 20 mM aniline and derivatives, 40 mM EDA, 10 mM dithionite, 1 h reaction time. Yields are based on GC/MS analysis.

Table 7. Results for the cyclopropanation reaction of styrene derivatives with YfeX R232A.


Substrate	Total Yield ^[a] (%)	TON	Cis:Trans
styrene	11	119 ± 12	11:89
styrene ^b	9	89 ± 12	7:93
4-methylstyrene	4	41 ± 5	23:77
vinylanisole	5	46 ± 10	14:86
4-chlorostyrene	5	50 ± 2	13:87

[a] Reaction conditions: 20 μM YfeX R232A (0.1 mol%), 20 mM styrene and derivatives, 40 mM EDA, 10 mM dithionite, 1 h reaction time. Yields are based on GC/MS analysis. [b] Reactions were run in 30% methanol.

results: although the reactivity for aniline and its *para*-substituted derivatives is similar to that of WT YfeX, there is a difference in the results for *ortho*-, *meta*-, and *para*-toluidine (see Table 6). These results suggest that R232 plays a subtle role in substrate orientation in the active site, influencing the reaction of the carbene intermediate with these bulkier substrates. When R232 is replaced by a smaller amino acid like Ala, the discrimination against the *ortho*- and *meta*-substituted compounds is eliminated, and similar yields are obtained for all toluidine substrates (see Table 6). In contrast, cyclopropanation reactions with YfeX R232A show no enhanced reactivity, but instead, a slight decrease of the yields is actually observed (see Table 7). To help increase styrene solubility in buffer, 30% methanol co-solvent was again used, similar to WT YfeX. This approach enhanced WT YfeX cyclopropanation reactivity, but unfortunately, this method did not improve catalysis with YfeX R232A. The reason for this became evident from circular dichroism (CD) spectroscopy. The CD data indicate that there is a subtle difference in protein folding between WT YfeX and YfeX R232A, with a slightly increased β-sheet contribution to the fold in the R232A variant (Figure S10). In addition, the folding of the variant is modified with increasing concentrations of methanol; this trend is not seen in WT YfeX where folding remains essentially unchanged for up to 50% methanol concentrations (Figure S8). These results indicate that YfeX R232A has a decreased stability compared to WT, and the structural changes that occur in the presence of methanol are counterproductive for catalysis. This part requires further study.

RuMpiX and CoPpiX Reconstituted YfeX

RuMpiX was prepared as previously described by Wolf et al. and reconstituted into YfeX.^[35] The Soret band of free [RuMpiX]⁺ at 389 nm shifts by 15 nm to lower energy after incorporation into the YfeX protein (Figure S4). Upon reduction of Ru(III)YfeX with Na₂S₂O₄, the Soret band sharpens and Q-bands appear at 495 and 520 nm, which is similar to Ru(II)Mb (Figure S4). The stability of both WT YfeX and RuYfeX under catalytic conditions was investigated by UV-vis spectroscopy. Most notably, after the addition of reductant and EDA to RuYfeX, a rapid decrease in the Soret band at 396 nm and the Q band at 521 nm occurs

(Figure S5). The decrease of the Soret band indicates that the porphyrin cofactor is modified over time, likely via intramolecular carbene transfer, as previously reported for RuMb.^[35] This likely leads to a rather fast decay of the reactivity of RuYfeX. Similarly, the Soret band of RuMb at 396 nm, corresponding to the carbene intermediate, decays over 1 h, with an initial decay of about half of the Soret band intensity over the first 20 minutes of the reaction with EDA.^[35]

The ability of RuYfeX to mediate carbene transfer reactions, N–H insertion and cyclopropanation, in buffer was further investigated as shown in Table 8. Activity toward the N–H insertion of aniline is similar between free [Ru^{II}MpIX], RuMb and variants,^[35] WT Mb and variants, and RuYfeX, with the latter achieving a 43 % yield (TON of 433) at pH 7. The N–H insertion of a secondary amine, *N*-methyl aniline, gave a somewhat lower yield of 39 % compared to aniline. Nevertheless, these numbers all pale in comparison to the N–H insertion activity of WT YfeX. Similar to Mb, the TONs decrease for the cyclopropanation of styrene upon RuMplX substitution into YfeX, giving a yield of 20 % for RuYfeX at pH 7, which is comparable to free [Ru^{II}MpIX] and WT Mb and variants. Notably though, the cyclopropanation activity of RuYfeX is greatly superior to RuMb.^[35] Styrene cyclopropanation with RuYfeX delivers a *cis* to *trans* ratio of 15 to 85, showing a higher *trans* selectivity compared to free [Ru^{II}MpIX], which yields a *cis* to *trans* ratio of 38 to 62.

Similarly, CoPpIX-reconstituted YfeX was characterized by UV-vis spectroscopy to show incorporation of the Co-porphyrin cofactor into YfeX. Co(III)YfeX shows the Soret band at 417 nm, with a shift to higher energy after reduction to the Co(II) form with dithionite to 398 nm (Figure S6). A CoYfeX carbene intermediate is generated upon addition of EDA to a solution of the protein, as shown by UV-vis spectroscopy, evident from a broadening and a concomitant shift of the Soret band to

393 nm. CoYfeX is able to facilitate carbene transfer reactivity at pH 7 in buffer for the N–H insertion of aniline, albeit only with 29 % yield (with a TON of 292), and for the cyclopropanation of styrene, the latter with a very small TON of only 49 (see Table 8). Previously, the Fasan group used the CoPpIX-reconstituted Mb(H64V, V68A) variant to analysis carbene transfer reactivity.^[55] Their results show that CoMb(H64V, V68A) has a lower reactivity for the N–H insertion than CoYfeX, with 13 % yield (and a TON of 129), but similar styrene cyclopropanation activity with 4 % yield.^[55] The catalytic activity of CoYfeX is relatively low compared to both WT YfeX and RuYfeX, and was therefore not further pursued.

MD and QM/MM Studies on the Si–H Insertion Reaction of YfeX

Since the Si–H insertion reaction is unusual and not fully understood, we undertook further computational studies to gain detailed insight into the energetics and the mechanism of this reaction, in the YfeX active site. In order to evaluate effects of the protein matrix as well, molecular dynamics and QM/MM studies were undertaken.

Conformational Flexibility of the YfeX-IPC Intermediate in the Presence of the Dimethylphenylsilane Substrate. Heme-protein catalyzed carbene insertion reactions have been reported to occur through a catalytic iron-porphyrin carbene (IPC) intermediate,^[38,52,54,56–58] which has been recently crystalized in the active site of *Rhodothermus marinus* (*Rma*) Cytochrome *c* by Arnold and co-workers.^[52] Since enzymes experience a broad range of internal motions that might be crucial for catalysis,^[59–61] we performed MD simulations of the reactive IPC intermediate in the presence of the substrate, dimethylphenylsilane, in the

Table 8. Carbene transfer reactivity of RuYfeX and CoYfeX.

Substrate	Catalyst	Yield ^[a] (%)	TON	Cis:Trans
aniline	[Ru ^{II} MpIX]	48	482 ± 11	
aniline	SW RuMb	36	360 ± 37	
aniline	RuYfeX	43	433 ± 21	
<i>N</i> -methyl aniline	RuYfeX	39	385 ± 60	
aniline	CoYfeX	29	292 ± 11	
<i>N</i> -methyl aniline	CoYfeX	5	49 ± 10	
aniline	CoMb(H64 V, V68 A) ^[b]	13	129	
styrene	[Ru ^{II} MpIX]	26	263 ± 121	38:62
styrene	SW RuMb	3	32 ± 12	20:80
styrene	RuYfeX	20	203 ± 56	15:85
styrene	CoYfeX	5	49 ± 16	15:85
styrene	CoMb(H64 V, V68 A) ^[b]	4	not reported	

[a] Reaction conditions: 20 μM YfeX derivative (0.1 mol%), 20 mM substrate, 40 mM EDA, 10 mM dithionite, 1 h reaction time. Yields are based on GC/MS analysis. [b] Based on studies by Sreenilayam et al.^[55]

active site (Figure 4a) to gain insight into its dynamical behavior and especially, the important interactions in the YFeX active site that might enhance the stability of the carbene intermediate and influence the orientation of the dimethylphenylsilane substrate. The protein complex is stable with an average root-mean-square deviation (RMSD) of 1.51 Å (Figure 4b), implying that the YfeX enzyme does not undergo huge conformational changes in the presence of the coordinated carbene group and the dimethylphenylsilane substrate, which are not naturally present in the enzyme's active site. The average distance between the carbene carbon atom and the Si atom of the substrate is 3.68 Å (Figure 4c), which is favorable for catalysis. The average N4–Fe–C1–C2 dihedral angle is found to be -95.2° , and this orientation of the carbene unit (relative to the heme) is stable (Figure 4d). This orientation of the carbene in the IPC with an N4–Fe–C1–C2 dihedral angle value of -90° has been reported in the captured IPC intermediate by Arnold and co-workers,^[52] which is consistent with our results with just a slight deviation due to the specific active site environment in YfeX.

The phenyl ring of the substrate orients parallel to one of the pyrrole rings of the heme in a manner favoring its stability by π -stacking (Figure S18), which is a key interaction that

stabilizes the substrate orientation in the IPC complex. Several SCS residues further stabilize both the substrate and the IPC in the active site. For example, the orientation of the substrate is further stabilized via both π -stacking and cation- π stacking interactions of its phenyl ring with the aromatic ring of F248 and with the guanidinium group of R232 (Figure S19), respectively. The salt-bridge interaction between R232 and one of the heme carboxylates enhances its favorable interactions with the substrate (Figure S19). Furthermore, the methyl groups of the substrate are stabilized by hydrophobic interactions with the methylene group of the S234 side chain and the ethyl group of the IPC carbene unit (Figure S18). Finally, the D143 side chain orients in such a way that its methylene group is locked in by hydrophobic interactions with the ethyl group of the IPC carbene unit (Figure S18). Networks of hydrogen bonding interactions between the axially ligating H215 and residues D274, S214, and L216, which are present in 69%, 39% and 31% of the MD trajectories, respectively, likely contribute to the stability of the complex. All these interactions play crucial roles in the stabilization of both the substrate and the IPC carbene unit and the proper orientation of the overall reactant complex. In particular, the IPC unit is firmly locked into this conformation,

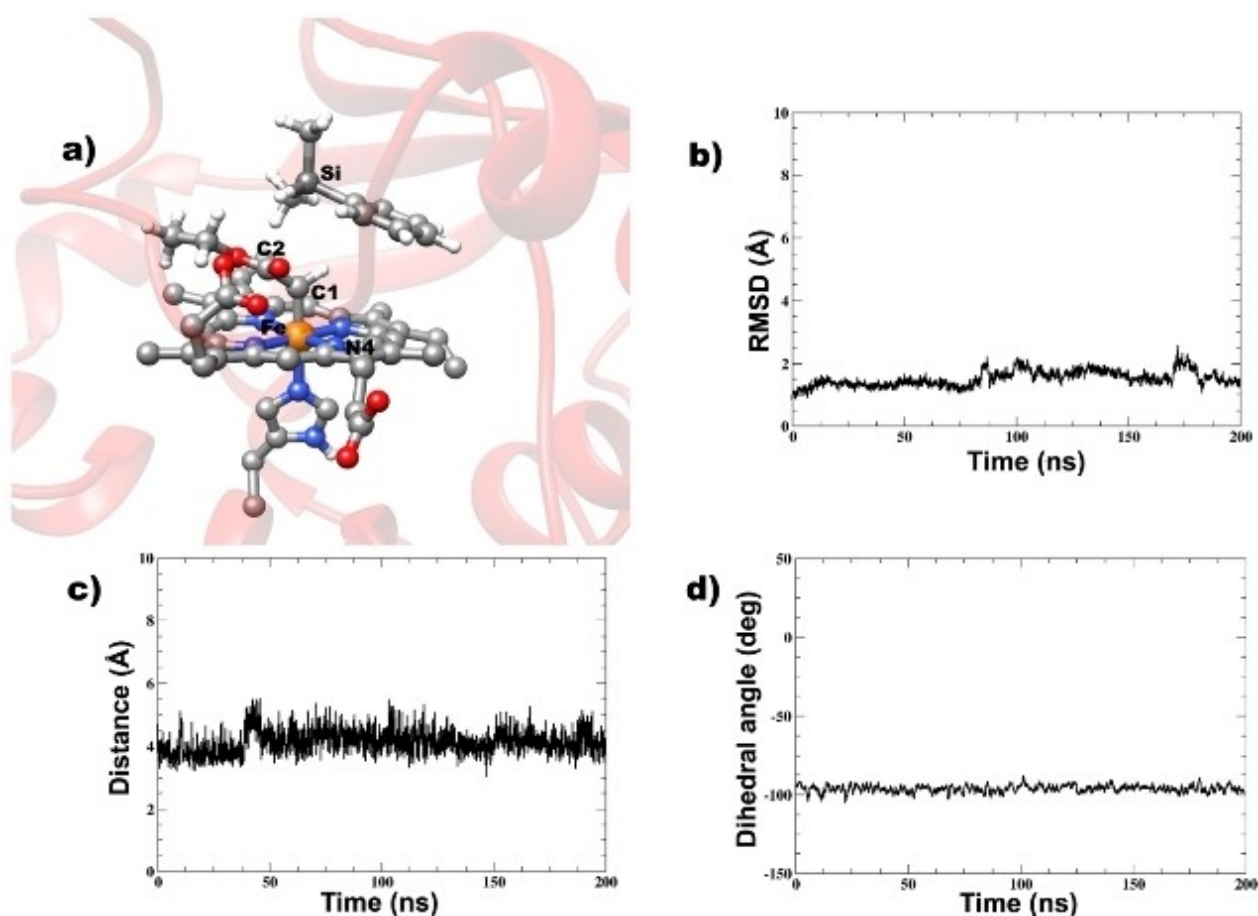


Figure 4. (a) Iron-porphyrin carbene (IPC) complex of YfeX with the substrate dimethylphenylsilane present in the active site. (b) Plot of RMSD for the YfeX IPC bound to dimethylphenylsilane substrate. (c) Plot of the distance between the carbene carbon (C1) and the substrate silicon (Si). (d) Plot of the N4–Fe–C1–C2 dihedral angle (see panel a) during the course of the simulation.

whereas the substrate shows some movement in the different trajectories.

QM/MM Calculations of the Reaction Mechanism of Si–H Insertion. In the carbene transfer reactions by iron porphyrin systems, the IPC intermediate has been reported to adopt three different spin states, namely the open-shell singlet (OSS), closed-shell singlet (CSS), and triplet state.^[52,54,56,62] To characterize the mechanism of carbene insertion into the Si–H bond of the substrate dimethylphenylsilane, we used combined QM/MM calculations using Turbomole^[63] and DL_POLY^[64] for QM and MM, respectively, as implemented in the ChemShell package.^[65] Interestingly, the QM/MM optimized IPC intermediates in the three spin states gave the triplet state at the lowest energy, 2.1 and 4.6 kcal/mol more stable than the OSS and CSS, respectively. In the optimized structures, the Fe–C1 bond distances in the triplet and OSS state are 1.92 and 1.86 Å, respectively, while a shorter bond distance of 1.79 Å is obtained in CSS. These structural parameters agree with earlier computational results; however, the question of the correct spin state of the IPC intermediate is still unclear.^[52,54,56,62,66] Computational studies that favor each one of these spin states as the ground state have been reported.^[36,54,56,58,66,67] However, the majority of studies have reported the OSS to be the lowest energy state.^[52,56,62,66] Furthermore, although this is still an open question, the protein environment might not affect the spin state energy order: a recent study, using both a QM cluster model and the QM/MM method, concluded that the spin state energy order is preserved in both cases for the studied system, independent of whether the protein environment is included or not.^[62] The process of Si–H insertion, involving partial hydride transfer from the silane to the carbene carbon and then the formation of a C–Si bond, passes through transition states TS_{OSS} , TS_{CSS} , and $TS_{triplet}$ for the OSS, CSS, and triplet spin states, respectively, with reaction barriers of 16.4, 22.8 and 27.6 kcal/mol, respectively. Hence, even though the triplet IPC has the lowest energy, our calculations reveal that the reaction coordinate requires a spin state crossing and that the reaction passing through TS_{OSS} is faster than the reactions through the other two transition states. TS_{OSS} is more favorable as it has the lowest barrier when compared to those observed for the other two spin states; therefore, TS_{OSS} is preferred over TS_{CSS} and $TS_{triplet}$. The computational results therefore point to a favorable OSS electronic spin state, in agreement with some previously reported computational findings.^[52,56,62,66] However, as discussed above, the nature of the most probable electronic ground state of the IPC intermediate is still a matter of discussion.

At the TS_{OSS} , the Fe–C1 and Si–H bonds elongate to 2.06 Å and 1.53 Å from 1.86 Å and 1.49 Å, respectively, while both the C1–Si and C1–H bonds shorten in readiness to form a new product involving the C1–Si bond, in agreement with previous computations.^[54,57,58] These bond distances are shorter for TS_{CSS} , as presented in Figure 5, than those obtained for the OSS and triplet spin states. Importantly, the transition state geometries are stabilized by several SCS residues. In TS_{OSS} , the guanidinium group of R232 forms a salt bridge with one of the heme carboxylates. Further, the phenyl ring of the substrate is stabilized by both π stacking and cation– π stacking interactions

with the phenyl ring of F248 and the guanidinium group of R232, respectively. These interactions are also conserved in the MD simulations. A network of hydrophobic interactions around the substrate and the carbene unit enhance the stabilization of the transition states. The methylene backbones of D137, D143 and F141 form hydrophobic interactions with the ethyl group of the carbene. The phenyl ring of F141 orients in a perpendicular manner to the heme ring and this π -stacking interaction thus locks its methylene backbone group in a position that favors the hydrophobic interaction with the ethyl moiety of the carbene unit. In addition, the methyl groups of the substrate are stabilized by the methylene group of the S234 backbone and the isobutyl side chain of L246, while the phenyl ring is stabilized by hydrophobic interactions with the R232 backbone methylene group as well as the hydrophobic environment created by the sec-butyl and methyl side chains of I230 and A250, respectively (Figure S15). The hydrophobic interactions observed for the ethyl group of the carbene are weaker in $TS_{triplet}$ and TS_{CSS} . Overall, all of these interactions contribute to the stabilization of the transition state. The transition states relax to products (PD_{OSS} , PD_{CSS} , and $PD_{triplet}$), where the C1–Si bond is fully formed and the Si–H bond is broken. The products formed in the three spin states are highly exothermic with energies of –77, –68, and –72 kcal/mol for PD_{OSS} , PD_{CSS} , and $PD_{triplet}$, respectively. Overall, the calculations show that the OSS state, which possesses the lowest transition state barrier of all the three spin states, is the most stable, implying that the formation of the C–Si bond product via the OSS spin state is both kinetically and thermodynamically favorable and preferred over the other spin states. The potential energy profile for the Si–H insertion reaction and the QM/MM-optimized stationary point geometries are presented in Figures 5 and S19.

Discussion

In this paper, we show that the enzyme YfeX is an excellent platform for further development of biocatalysts for carbene transfer reactions. Such carbene transferases are of particular interest for late-stage functionalization of drug precursors, allowing for the efficient synthesis of pharmaceuticals. These enzymes have the ability to form new C–C and C-heteroatom bonds under mild reaction conditions, where the tuning of the enzyme active site and beyond enables stereo- and even enantioselective reactions to be performed.^[1–7] So far, Cyt. P450s and myoglobin (Mb) have mainly served as the work horses for the development of carbene transferases.^[34,68,69] However, the catalytic activity of WT Mb, for example, is somewhat limited. As pointed out by Arnold, for the development of robust biocatalysts it is of advantage to start from a WT enzyme that itself has a high catalytic activity for a desired transformation.^[29] As we show in this work, the peroxidase YfeX is an excellent platform for further biocatalyst development, by either directed evolution and/or rational design. In particular, WT YfeX shines with high catalytic activity for the N–H insertion of aromatic and aliphatic primary and secondary amines that is comparable to those of the best Mb mutants available to this

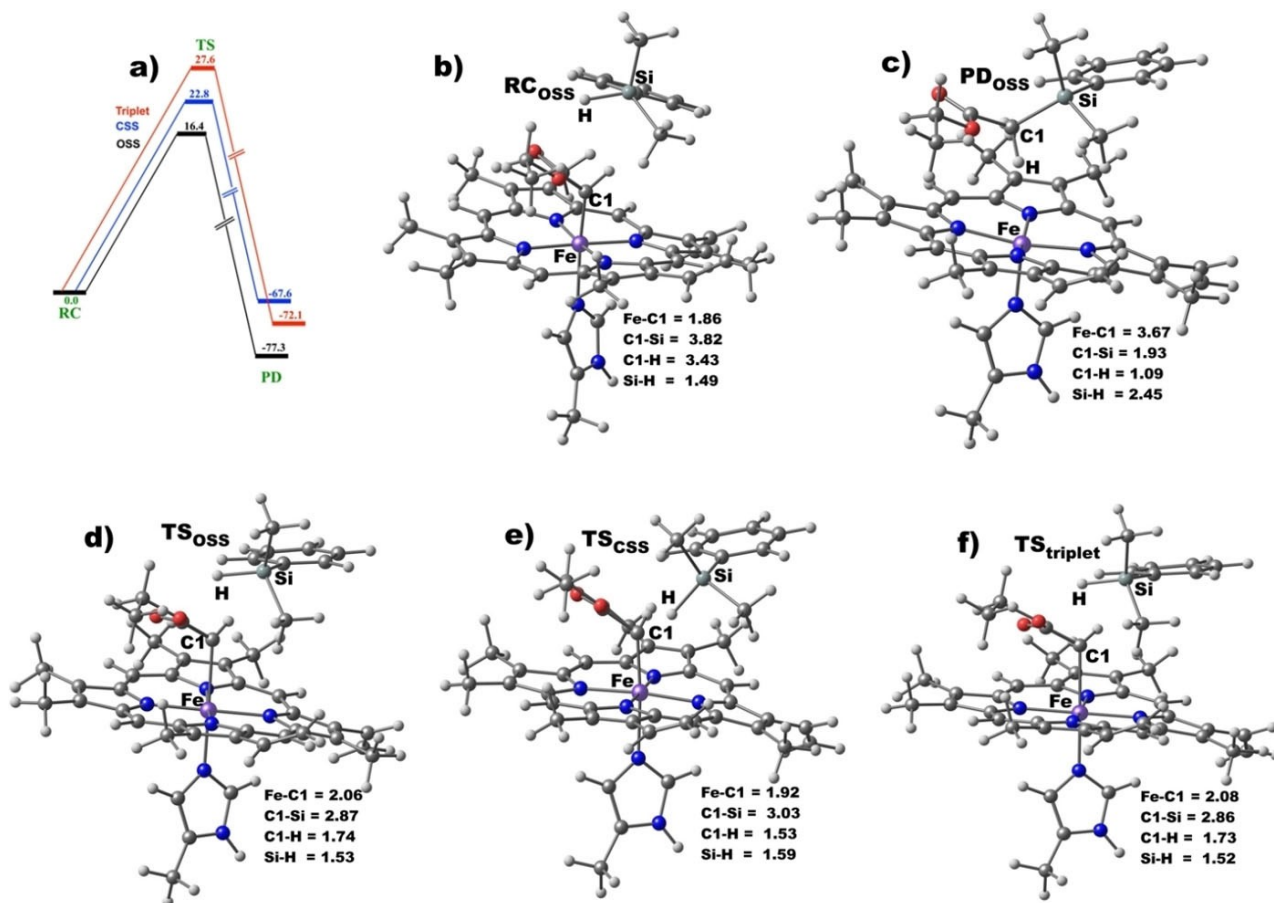


Figure 5. (a) QM/MM potential energy profile for Si–H insertion catalyzed by YfeX-IPC, calculated at the BS2 + ZPE level of theory. (b–c) Geometries of the reactant and product complexes for the OSS state, and (d–f) geometries of the transition states in the OSS, CSS and triplet spin states. The relative energies in (a) are in kcal/mol while the distances in (b–f) are in Å.

date from the Fasan group.^[51] For example, WT YfeX has a 70% yield (at 0.1 mol% catalyst loading in just 1 h), and up to a TON of >6000 (at 0.001 mol% loading after 20 h) for the N–H insertion of aniline with EDA. Curiously, the cyclopropanation activity of YfeX, on the other hand, is comparable to that of Mb. As we show in this work, this is largely due to the lack of solubility of the corresponding test substrate, styrene, in buffer, and its inability to access the YfeX active site. So, whereas the intrinsic reactivity of the central carbene intermediate seems to be much higher in YfeX, Mb seems to profit from easier access to its heme cofactor (due to the lack of a real active site pocket) when substrates are used that lack water solubility. However, YfeX also shows remarkable stability in organic solvents, and in the presence of 30% methanol to improve styrene solubility, the yield for the cyclopropanation of styrene by WT YfeX increases to 47%. Under similar conditions, benzylamine gives a 56% yield for N–H insertion. Other styrene and aniline derivatives were tested as well, giving excellent yields for carbene transfer reactions, as shown in Tables 3 and 4. Even more impressively, WT YfeX is able to catalyze the Si–H insertion of dimethylphenylsilane with 11% yield (at 0.1 mol% catalyst loading in just 1 h), which is superior to other WT proteins studied so far.^[29,54,58] These results show that YfeX (and

potentially other peroxidases) has great potential to become the next universal work horse for the development of a broad range of new carbene transferases, given its high intrinsic reactivity for carbene transfer reactions. A basic comparison between the reactivity of WT Mb and WT YfeX is given in Table 9.

To explore the substrate scope of YfeX for the N–H insertion and cyclopropanation reaction, a variety of *para*-substituted anilines and styrenes with electron-donating and electron-

Table 9. Product yield comparison between WT Mb and WT YfeX for standardized test substrates. All WT YfeX data were obtained at 0.1 mol% catalyst loading.

Substrate	Wt Mb	Time	Wt YfeX	Time
styrene	36% ^[b]	16 h	27%	1 hr
			59% ^[a]	
aniline	21% ^[c]	12 h	72%	1 hr
benzylamine	17% ^[d]	16 h	56% ^[a]	1 hr
dimethylphenyl-silane	35% ^[e]	12 h	11%	1 hr

[a] Using 30% DMSO (styrene) or 30% MeOH (benzylamine) as co-solvent. [b] Data from ref. [23] using 0.2 mol% Mb. [c] Data from ref. [50] using 0.2 mol% Mb. [d] Data from ref. [51] using 0.2 mol% Mb. [e] Data from ref. [53] using 0.2 mol% Mb.

withdrawing substituents were subjected to reactivity with EDA. Similar to previous results with Mb and P450s,^[3,7,8,51,70] it was shown that YfeX favors electron-rich substrates. The enhanced preference to electron-rich substrates is due to their higher reactivity toward the electrophilic heme-carbene intermediate that facilitates these reactions.^[7,8,52,70] Moreover, YfeX cyclopropanation reactivity shows that it can generate the *trans* product in high yield with 87% selectivity for the (R,R) enantiomer, unlike WT Mb, which produces 47% (R,R) enantiomer.^[23] It has been shown that SCS interactions play a major role in diastereo- and enantioselectivity for cyclopropanation reactivity,^[7,57,62] therefore, differences in selectivity for WT YfeX compared to WT Mb are likely due to SCS variations near the heme active site. This point requires further investigation. Fasan and coworkers have further explored cyclopropanation selectivity using crystallographic, computational, and reactivity/mutagenesis studies in Mb and mutants.^[57] They highlight the importance of steric complementarity and noncovalent interactions to guide stereochemical selectivity during cyclopropanation reactivity, and corresponding studies on YfeX are currently in progress.^[57]

In Mb, key improvements in carbene transfer catalysis were achieved by substitution of the distal His with smaller amino acids. In YfeX, R232, a positively charged amino acid that could interact with the carbene intermediate and/or the substrates, is located right above the heme plane (5.9 Å away from the heme). Due to its location within the active site, this amino acid could therefore have a direct effect on reactivity. To investigate this point further, the YfeX mutant R232A was generated. Work on YfeX R232A shows that for N–H insertion, an overall similar reactivity is observed for aniline and its *para*-substituted derivatives as in the case of WT enzyme, so the R232 residue is flexible enough (in contrast to the distal His in Mb) to not impact overall carbene transfer reactivity significantly. However, a change in selectivity is observed for the toluidine derivatives, with enhanced reactivity towards *ortho*- and *meta*-toluidine, indicating that R232 does impact substrate orientation in the active site for bulkier molecules. Interestingly, a slight decrease in yield is observed for cyclopropanation with YfeX R232A. This is in agreement with the proposal that access into the active site is the major hindering factor for cyclopropanation with YfeX (see above), so the R232A mutation only has a small impact on catalysis. We further show that YfeX R232A is not as stable as WT YfeX and this could contribute to the lower reactivity.

We further investigated if an improvement of catalytic activity of YfeX could be achieved using other transition metals. For this purpose, we reconstituted YfeX with Co- and Ru-heme cofactors, which have shown promise for improving carbene transfer reactivity for Mb.^[35,71] However, in the case of YfeX, no improvements in carbene transfer activity are observed with these cofactors. In agreement with these findings, the previously noted instability of RuMb persists for RuYfeX, emphasizing that carbene insertion into the porphyrin ring is a general reactivity feature of (biological) Ru-hemes, which would otherwise be highly active catalysts.^[35] Therefore, the cheapest metal, iron, turns out to also give the most active and robust catalyst of all transition metals tested thus far with YfeX.

Since the Si–H insertion reaction is unique, we investigated this reaction further using computational methods. Whereas many WT heme proteins are able to catalyze the N–H insertion or cyclopropanation reaction, albeit often with very low yields, the Si–H reaction is much more challenging, and there are very few WT heme proteins that are able to mediate this process efficiently.^[29] Here, we investigated this reaction starting from the three possible electronic ground states of the iron-porphyrin carbene (IPC) intermediate, which are the closed shell singlet (CSS) and open shell singlet (OSS) state, and the corresponding triplet state. As observed previously, these three states are very close in energy (within 5 kcal/mol), making it impossible to determine which form corresponds to the ground state of the IPC based solely on the computational results.^[52,70] Previous studies on truncated DFT models indicated that there is no energy barrier for either the N–H insertion and cyclopropanation reactions, but there is a free energy barrier due to the entropic contribution, corresponding to 9–14 kcal/mol.^[57,66] In contrast, for the Si–H insertion by YfeX, the calculated energy barriers are 16.4 (OSS), 22.8 (CSS) and 27.6 (triplet) kcal/mol, indicating that the OSS state is ultimately allowing for this reaction to go forward. Overall, these results show that the Si–H insertion reaction is energetically much less favorable compared to the N–H insertion and cyclopropanation reactions, in agreement with the lack of reactivity of many WT heme proteins towards carbene transfer to Si–H bonds.

As shown by our results, the YfeX active site is uniquely equipped to stabilize the transition state for the Si–H insertion with dimethylphenylsilane, by locking the IPC complex and the substrate into a conformation that is productive for catalysis. During the MD simulations, the orientation of the substrate relative to the IPC intermediate shows little variation, thereby promoting this reaction despite the rather large activation barrier. Recently, Arnold, Houk and coworkers investigated the Si–H insertion reaction as catalyzed by the *Rma* Cyt. *c* V75T M100D M103E triple variant (termed “*Rma* TDE”) through experimental and computational studies.^[54] They determined that *Rma* TDE catalyzes carbene insertion into Si–H bonds through a concerted, nonradical mechanism, and in their DFT and QM/MM calculations, the CSS is the most favorable transition state.^[54] The transition state energies obtained from their QM/MM studies are rather similar to the ones obtained by us for YfeX, again emphasizing that YfeX is intrinsically suited for the Si–H insertion reaction, and thus, has the potential to be further optimized for this reaction to achieve high turnover numbers. Similarly, Fasan, Zhang and coworkers investigated the Mb-catalyzed carbene insertion into Si–H bonds, using a truncated DFT model for the calculations and radical trap experiments. Based on their results, it was concluded that the carbene insertion into Si–H bonds occurs through a concerted mechanism involving a CSS transition state.^[58] As discussed above, our calculations predict that in the case of YfeX, the mechanism of Si–H insertion with dimethylphenylsilane involves an OSS transition state rather than a CSS transition state, as found for *Rma* TDE and Mb. These differences could be related to variations within the active sites of these proteins. Figure 6 compares the electrostatic potential surface maps for

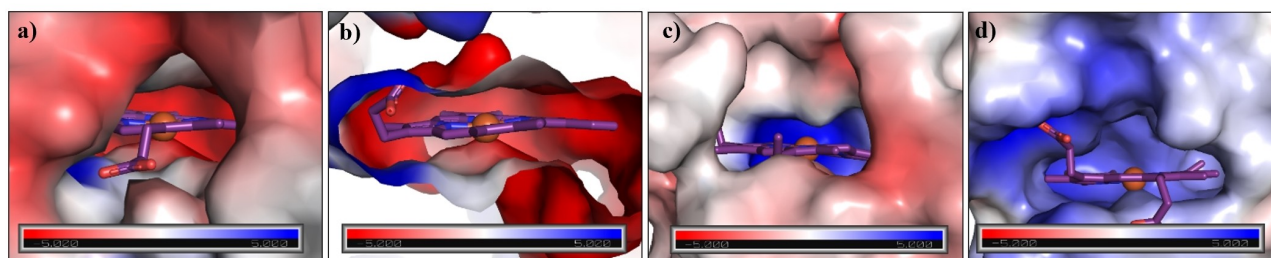


Figure 6. Electrostatic potential surface for the active site of (a) YfeX (PDB code 2IZ) from the outside, and (b) zoomed-in version for YfeX, (c) *Rma* TDE (PDB code 6CUN), and (d) Mb (H64V, V68A) (PDB code 6M8F). Electrostatic potential surfaces were drawn in PyMOL using APBS electrostatics (the red color corresponds to negative potential and the blue color corresponds to positive potential).

the active sites of YfeX, *Rma* TDE, and Mb (H64V, V68A; one of the most active Mb-based carbene transfer catalysts), indicating key differences in YfeX compared to these other catalysts. Whereas YfeX has a polar active site with both negatively and positively charged regions, and a narrow tunnel that leads into the active site, both *Rma* TDE and Mb (H64V, V68A) have much more open active sites with neutral to positive electrostatic potential. This explains why YfeX has intrinsically a high reactivity for N–H insertion, where polar aniline has a relatively high affinity for the active site of YfeX, whereas non-polar styrene does not. Styrene cyclopropanation is therefore drastically enhanced in the presence of organic co-solvents that help improve the availability of this substrate in solution for WT YfeX, whereas for aniline, the effect of an organic co-solvent is small. In addition, YfeX is able to better confine dimethylphenylsilane in the active site, which promotes reactivity. As evident from Figure 6, YfeX clearly contrasts with *Rma* TDE and Mb (H64V, V68A) with respect to its active site properties, which again emphasizes the great potential of YfeX and other peroxidases to access unprecedented reactivity space in biocatalytic transformations. Investigations in this regard are ongoing.

Conclusion

In conclusion, our results show that YfeX is a highly reactive and versatile catalyst for carbene transfer reactions, and in its WT form, shows excellent reactivity for the reactions we explored here, compared to WT Mb and diverse WT Cyt. P450s. In addition, the protein shows high stability against organic solvents, thereby enabling the use of organic co-solvents whenever necessary in order to improve turnover for hydrophobic substrates. Utilizing MeOH and DMSO co-solvents we show that cyclopropanation reaction yields significantly increase for WT YfeX, overcoming some of the low solubility barrier faced by styrene in aqueous buffer. The rather large active site of YfeX further promises exciting applications of this protein in the synthesis of pharmaceuticals and fine chemicals, allowing for the processing of rather large substrates, especially after (potentially) opening up the tunnel into the active site via site-directed mutagenesis. Such studies are in progress, com-

pared with site-directed mutagenesis studies that aim to explore the role of important second coordination sphere groups in the YfeX active site during various carbene transfer reactions. YfeX is an exciting new target for the design of new carbene transferases, with many potential applications in the pharmaceutical industry in the future.

Experimental Section

General Procedures: All chemicals and reagents were purchased from commercial suppliers (Sigma-Aldrich, Fisher Scientific, Acros, Frontier Scientific) and used without further purification unless otherwise noted. UV-visible spectra were recorded on an Analytic Jena Specord S600 spectrophotometer using sealed quartz cuvettes. ^{13}C - and ^1H -NMR spectra were measured on either a Varian MR400 (operating at 400 MHz), a Varian Inova 500 (operating at 500 MHz), or a Varian V NMRS 500 (operating at 500 MHz). Tetramethylsilane (TMS) served as the internal standard (0 ppm) for ^1H -NMR measurements.

Gas chromatography/mass spectrometry (GC/MS) analyses were performed using a Shimadzu QP-2010 GC/MS equipped with a 30 m long DB-5 column with 0.25 mm ID. Separation method: 1 μL injection, injector temperature: 200 °C, detector temperature: 250 °C. Gradient: column temperature set to 60 °C for 3 min, then to 250 °C at 20 °C min^{-1} and held at 250 °C for 2.5 min (7.5 min for derivatives). Total run time was 15.00 min for the aniline and styrene reactions, and 20.00 min for the reactions with the aniline and styrene derivatives.

Supercritical fluid chromatography (SFC) used to resolve the enantiomer products for cyclopropane compounds was performed using a Waters SFC instrument equipped with a column oven (35 °C), photodiode array detector, a backpressure regulator (12.0 MPa), a carbon dioxide pump and a sample injection volume of 3 μL . A Daicel Chiralpak IC column (5 μm , 4.6 \times 250 mm analytical chiral column) was used for separation of the enantiomers and % ee determination. All samples were eluted using an isocratic solvent system with the indicated modifier in liquid CO_2 , containing 10% isopropanol as co-solvent, at an elution rate of 4 mL/min and detection at $\lambda = 250$ nm with a total run time of 6.0 min.

YfeX and YfeX R232A Protein Expression, Purification: Protein expression and purification followed a protocol by the Weissenborn group (Martin-Luther-University Halle-Wittenberg in Halle (Saale), Germany).^[49] The YfeX genes (pCA24 N) were transformed into chemocompetent *E. coli* BL21 (DE3) cells by heat shock. Freshly plated transformants were grown overnight in 5 ml Terrific Broth

(TB) medium containing 50 µg/ml chloramphenicol. 2 ml of the pre-cultures were inoculated in 400 ml TB autoinduction medium containing 50 µg/ml chloramphenicol. Cells were incubated at 37 °C and 120 rpm. After 4 h of cultivation, aqueous solutions of FeCl₃/5-aminolevulinic acid (final concentration: 100 µM) were added, the temperature was reduced to 30 °C and the cells were incubated for further 16.5 h. Cells were harvested by centrifugation (3000×g, 20 min, 4 °C). The supernatant was discarded, and the pellets were resuspended in binding buffer (50 mM KPi, pH=7.4, 200 mM NaCl). Cells were lysed by sonication (Bandelin Sonoplus HD3100: 6×30 s, 70% amplitude, pulse mode) and the lysate was incubated with hemin (final concentration: 600 µM) at room temperature for 30 min with a final DMSO concentration of 2%. The cell debris was removed by centrifugation for 45 min at 4 °C and 6000×g. Excess of hemin and traces of DMSO were removed during the protein purification steps. The protein exhibits a hexahistidine-tag and was purified by IMAC (immobilized metal ion affinity chromatography) using 1 mL His GraviTrap TALON columns (GE Healthcare Europe GmbH, Freiburg, DE). Washing buffer consisting of 50 mM Kpi (pH=7.4), 200 mM NaCl and 5 mM imidazole was used to remove unspecific proteins. Protein was finally eluted by the addition of elution buffer (50 mM Kpi (pH=7.4), 200 mM NaCl and 250 mM imidazole). PD-10 desalting columns (GE Healthcare Europe GmbH, Freiburg, DE) were used for buffer exchange of the pooled elution fractions, yielding the purified protein in 50 mM KPi (pH=7.4) and 10% glycerol (v/v). These stocks were flash-frozen in liquid N₂ and stored at -20 °C. Protein and heme *b* amounts were determined in duplicates using the BSA Protein Assay and the Pyridine Hemochromagen Assay (reduced form, $\epsilon = 34.7 \text{ mM}^{-1} \text{ cm}^{-1}$ at 557 nm).

Protein mass spectrometry analyses were performed using an Agilent Q-TOF HPLC-MS equipped with a Poroshell 300SB-C8 column. Separation method: 20 µL injection, flow rate: 0.5 mL/min, gradient: 95:5 water/acetonitrile for 3 min, followed by an increase over 10 min to 100% acetonitrile to elute the protein. Total run time was 13 min. Porphyrin mass spectrometry analyses were performed using an Agilent 6230 TOF HPLC-MS.

N–H Insertion Reactions: Reactions were performed as previously described,^[35] at a ~450 µL scale using 20 µM YfeX, 20 mM aniline (or aniline derivative), 40 mM ethyl diazoacetate (EDA), and 10 mM Na₂S₂O₄. The sodium dithionite (100 mM stock solution) in potassium phosphate buffer (100 mM, pH 7.0) was purged by bubbling nitrogen through the solution for 10 min in a sealed vial. All reagents and proteins were brought into a Coy vinyl anaerobic chamber (10–30 ppm of O₂, 1.5–3.0% H₂) before running the reactions. The as-isolated, ferric YfeX was first reduced to ferrous YfeX through addition of 40 µL of Na₂S₂O₄ solution, followed by the addition of 4 µL of aniline or aniline derivatives from a 2 M stock solution in methanol, and 8 µL of EDA (2 M stock solution in methanol), which translates to a total MeOH content of 2.65%. The reactions were left under magnetic agitation for 1 h at room temperature (or as indicated).

Cyclopropanation Reactions: Reactions were performed in the same manner as the N–H insertion reactions, using 20 mM styrene (or styrene derivatives) instead of aniline. All 2 M styrene solutions were prepared in methanol.

Si–H Insertion Reactions: Reactions were performed in the same manner as the N–H insertion reactions, using 20 mM dimethylphenylsilane (or silane derivatives) instead of aniline. All 2 M silane solutions were prepared in methanol.

Product Analysis: The reactions were analyzed, as previously described,^[15] by addition of 20 µL of internal standard (2-phenylethanol, 1 M in methanol) to the reaction mixture, followed by extraction with 1.5 or 3 mL of ethyl acetate, depending on the

reaction. The organic layers were dried with magnesium sulfate and later filtered and analyzed by GC/MS and SFC (see General Procedures section for details on GC/MS and SFC analyses). Calibration curves for quantification of the N–H insertion products of aniline and aniline derivatives and the cyclopropanation products of styrene and styrene derivatives were constructed using authentic standards produced synthetically (using 1–2 mol% Rh₂(OAc)₄ as the catalyst). These products were used to generate calibration curves for quantification of the aniline and styrene products in the catalytic reactions with YfeX. The reactions to produce authentic standards were conducted according to the same methods previously reported by our laboratory.^[35] All measurements reported in the Results tables were performed in triplicate. Negative control experiments were performed in the absence of YfeX.

Computational Methods: System Preparation and MD Simulation:

The initial coordinates of the system were generated using an X-ray crystal structure of YfeX (PDB code: 5GT2).^[47] The precursor for the iron porphyrin carbene (IPC) intermediate and the dimethylphenylsilane substrate were modelled in the active site using GaussView 6.0.^[72] The protonation states of the ionizable side chains were accessed with Propka software,^[73] while the axial His215 that is coordinated to the Fe center of the heme was assigned a protonation state based on visual inspection of its local environment. The active center parameters were generated using Metal Center Parameter Builder (MCPB.py),^[74] as implemented in Amber18. The bond and angle force constants were derived using the Seminario method,^[75] while point charge parameters for the electrostatic potentials were obtained using the ChgModB method. The parameters for the carbene precursor complex and the silane substrate were generated using the Antechamber module of Amber18.^[76] All the missing hydrogen atoms in the crystal structure were added with the Leap module in Amber and charges were neutralized using Na⁺ counterions. The system was solvated with TIP3P water molecules in a rectangular box within a distance of 10 Å from the protein's surface.^[77] Several MD and QM/MM studies on both heme and non-heme Fe containing enzymes have successfully used the parameters generated via this procedure to study both the dynamics and the catalytic mechanism of the Fe containing systems.^[52,54,78,79]

A two-stage minimization of the geometries was first performed using MM to eliminate clashes of atoms. In the first stage of minimization, only the water molecules and the Na⁺ counterions were minimized, while the solute molecules were restrained with a harmonic potential of 500 kcal/(molÅ²). In the last minimization stage, all the atoms were geometrically optimized without any restraint. The system was subjected to 5000 steps of steepest descent, followed by 5000 steps of conjugate gradient energy minimization. The minimized system was first slowly heated from 0 to 300 K for 50 ps in an NVT ensemble using a Langevin thermostat.^[80] The heated system was further subjected to constant temperature heating at 300 K for 1 ns in an NPT ensemble. The solute molecules were restrained with a harmonic potential of 10 kcal/(molÅ²) during all the heating processes. After that, the system was equilibrated for 3 ns in an NPT ensemble at a fixed temperature and pressure of 300 K and 1 bar, respectively, without any restraints on solute molecules. After equilibration, a restrained productive MD was then run for 200 ns using the distance NMR refinement module in Amber18 by restraining the distance between the Si atom of the silane substrate and the carbene carbon from 2.8 and 3.5 Å, followed by an unrestrained productive MD for another 200 ns in an NPT ensemble with a target pressure set at 1 bar and constant pressure coupling of 2 ps.^[81] The pressure was held constant using Brendsen barostat^[82] and the SHAKE algorithm^[83] was used to constrain the bond lengths of those bonds

involving hydrogen atoms. The simulations were performed using the GPU version of the PMEMD engine integrated in Amber18.^[84] The Amber FF14SB force field was used for the simulations,^[85] and periodic boundary conditions were employed. The obtained trajectories were processed and analyzed using the CPPTRAJ module from AmberTools utilities.^[86]

QM/MM Calculations: QM/MM calculations were performed with the ChemShell program,^[65] which combines Turbomole^[63] for the QM region and DL_POLY^[64] for the MM region. The electrostatic embedding scheme was used to describe the interactions between the two regions, while hydrogen link atoms were used to treat the boundary between the QM and the MM region. The QM region was represented using the UB3LYP functional with the 6-31G(d) basis set for all atoms except Fe where the LANL2DZ basis set with an effective core potential (ECP; labeled BS1) was used, as in previous, similar studies on carbene transfer reactions.^[56,57,66,87] The MM region was described with the Amber force field. The QM region consists of the Fe-porphyrin carbene intermediate, dimethylphenylsilane and the methylene imidazole group of the axial His215 ligand. After the initial QM/MM geometry optimization, linear transit scans along the reaction coordinate were performed with 0.1 Å increment to obtain the transition states using a DL_find optimizer.^[88] The transition states were reoptimized using the P-RFO algorithm implemented in the HDLC optimizer.^[89] The fully optimized geometries of the minima and the transition states were characterized via frequency calculations. The final energies of the optimized stationary points were recomputed via single-point energy calculation using the all electron def2-TZVP basis set (labeled BS2) for all atoms. To obtain the open-shell singlet state (OSS) structures, the optimized triplet state structure was used as a starting point, followed by flipping one α -electron to a β -electron, and then an unrestrained geometry optimization was performed on this structure. To do the spin flip, the 'flip' module in Turbomole was used.

Acknowledgements

Financial support for this work from the University of Michigan, Associate Professor Support Fund, is gratefully acknowledged (to NL). VSA acknowledges support from a Rackham Merit Fellowship and a Robert W. Parry Scholarship (both University of Michigan). CZC acknowledges the funding from NSF grant 1904215 and NIH grant 1R15GM139118-01A1 for testing the computational methodology.

Conflict of Interest

The authors declare no conflict of interest.

Data Availability Statement

The data that support the findings of this study are available from the corresponding author upon reasonable request.

Keywords: biocatalysis · carbene transfer · cyclopropanation · N–H insertion · QM/MM calculations

- [1] X. Lim, *Nature News* **2016**, 537, 156.
- [2] H. Renata, Z. J. Wang, R. Z. Kitto, F. H. Arnold, *Catal. Sci. Technol.* **2014**, 4, 3640–3643.
- [3] Z. J. Wang, N. E. Peck, H. Renata, F. H. Arnold, *Chem. Sci.* **2014**, 5, 598–601.
- [4] J. A. McIntosh, P. S. Coelho, C. C. Farwell, Z. J. Wang, J. C. Lewis, T. R. Brown, F. H. Arnold, *Angew. Chem. Int. Ed.* **2013**, 52, 9309–9312; *Angew. Chem.* **2013**, 125, 9479–9482.
- [5] P. S. Coelho, E. M. Brustad, A. Kannan, F. H. Arnold, *Science* **2013**, 339, 307–310.
- [6] P. S. Coelho, Z. J. Wang, M. E. Ener, S. A. Baril, A. Kannan, F. H. Arnold, E. M. Brustad, *Nat. Chem. Biol.* **2013**, 9, 485–487.
- [7] M. Bordeaux, V. Tyagi, R. Fasan, *Angew. Chem.* **2015**, 127, 1764–1768; *Angew. Chem. Int. Ed.* **2015**, 54, 1744–1748.
- [8] Y. Wei, A. Tinoco, V. Steck, R. Fasan, Y. Zhang, *J. Am. Chem. Soc.* **2017**, 140, 1649–1662.
- [9] K. Shanab, C. Neudorfer, E. Schirmer, H. Spreitzer, *Curr. Org. Chem.* **2013**, 17, 1179–1187.
- [10] I. Nicolas, T. Roisnel, P. Le Maux, G. Simonneaux, *Tetrahedron Lett.* **2009**, 50, 5149–5151.
- [11] F. P. Caló, A. Zimmer, G. Bistoni, A. Fürstner, *J. Am. Chem. Soc.* **2022**, 144, 7465–7478.
- [12] D. Sinou, *Metal catalysis in water*, Springer **1999**.
- [13] I. T. Horvath, P. T. Anastas, *Chem. Rev.* **2007**, 107, 2169–2173.
- [14] A. Birch, D. Williamson, *Org. React.* **2004**, 24, 1–186.
- [15] G. C. Vougioukalakis, R. H. Grubbs, *Chem. Rev.* **2010**, 110, 1746–1787.
- [16] P. Eilbracht, L. Bäracker, C. Buss, C. Hollmann, B. E. Kitsos-Rzychon, C. L. Kranemann, T. Rische, R. Roggenbuck, A. Schmidt, *Chem. Rev.* **1999**, 99, 3329–3366.
- [17] D. L. Purich, *Enzyme kinetics: catalysis and control: a reference of theory and best-practice methods*, Elsevier **2010**.
- [18] B. Hauer, *ACS Catal.* **2020**, 10, 8418–8427.
- [19] S. Chakrabarty, Y. Wang, J. C. Perkins, A. R. Narayan, *Chem. Soc. Rev.* **2020**, 49, 8137–8155.
- [20] R. A. Sheldon, D. Brady, *Chem. Commun.* **2018**, 54, 6088–6104.
- [21] K. Chen, F. H. Arnold, *Nat. Catal.* **2020**, 3, 203–213.
- [22] B. J. Wittmann, A. M. Knight, J. L. Hofstra, S. E. Reisman, S. Jennifer Kan, F. H. Arnold, *ACS Catal.* **2020**, 10, 7112–7116.
- [23] P. Bajaj, G. Sreenilayam, V. Tyagi, R. Fasan, *Angew. Chem.* **2016**, 128, 16344–16348; *Angew. Chem. Int. Ed.* **2016**, 55, 16110–16114.
- [24] M. J. Weissenborn, R. M. Koenigs, *ChemCatChem* **2020**, 12, 2171–2179.
- [25] Z. Liu, F. H. Arnold, *Curr. Opin. Biotechnol.* **2021**, 69, 43–51.
- [26] R. Stenner, J. W. Steventon, A. Seddon, J. R. Anderson, *Proc. Nat. Acad. Sci.* **2020**, 117, 1419–1428.
- [27] R. A. Sheldon, D. Brady, *ChemSusChem* **2019**, 12, 2859–2881.
- [28] M. J. Hernáiz, A. R. Alcántara, J. I. García, J. V. Sinisterra, *Chem. Eur. J.* **2010**, 16, 9422–9437.
- [29] S. J. Kan, R. D. Lewis, K. Chen, F. H. Arnold, *Science* **2016**, 354, 1048–1051.
- [30] Y.-W. Lin, N. Yeung, Y.-G. Gao, K. D. Miner, S. Tian, H. Robinson, Y. Lu, *Proc. Nat. Acad. Sci.* **2010**, 107, 8581–8586.
- [31] M. Tegoni, F. Yu, M. Bersellini, J. E. Penner-Hahn, V. L. Pecoraro, *Proc. Natl. Acad. Sci. USA* **2012**, 109, 21234–21239.
- [32] M. Sono, M. P. Roach, E. D. Coulter, J. H. Dawson, *Chem. Rev.* **1996**, 96, 2841–2887.
- [33] A. Tinoco, V. Steck, V. Tyagi, R. Fasan, *J. Am. Chem. Soc.* **2017**, 139, 5293–5296.
- [34] O. F. Brandenburg, R. Fasan, F. H. Arnold, *Curr. Opin. Biotechnol.* **2017**, 47, 102–111.
- [35] M. W. Wolf, D. A. Vargas, N. Lehnert, *Inorg. Chem.* **2017**, 56, 5623–5635.
- [36] K. Oohora, H. Meichin, L. Zhao, M. W. Wolf, A. Nakayama, J.-y. Hasegawa, N. Lehnert, T. Hayashi, *J. Am. Chem. Soc.* **2017**, 139, 17265–17268.
- [37] P. Dydio, H. Key, A. Nazarenko, J.-E. Rha, V. Seyedkazemi, D. Clark, J. Hartwig, *Science* **2016**, 354, 102–106.
- [38] T. Hayashi, M. Tinzl, T. Mori, U. Krengel, J. Proppe, J. Soetbeer, D. Klose, G. Jeschke, M. Reiher, D. Hilvert, *Nat. Catal.* **2018**, 1, 578–584.
- [39] G. Sreenilayam, E. J. Moore, V. Steck, R. Fasan, *ACS Catal.* **2017**, 7, 7629–7633.
- [40] A. L. Chandgude, X. Ren, R. Fasan, *J. Am. Chem. Soc.* **2019**, 141, 9145–9150.
- [41] D. A. Vargas, A. Tinoco, V. Tyagi, R. Fasan, *Angew. Chem. Int. Ed.* **2018**, 57, 9911–9915; *Angew. Chem.* **2018**, 130, 10059–10063.
- [42] D. M. Carminati, J. Decaens, S. Couve-Bonnaire, P. Jubault, R. Fasan, *Angew. Chem. Int. Ed.* **2021**, 60, 7072–7076.

- [43] L. Villarino, K. E. Splan, E. Reddem, L. Alonso-Cotchico, C. Gutiérrez de Souza, A. Lledós, J. D. Maréchal, A. M. W. Thunnissen, G. Roelfes, *Angew. Chem. Int. Ed.* **2018**, *57*, 7785–7789; *Angew. Chem.* **2018**, *130*, 7911–7915.
- [44] A. M. Knight, S. J. Kan, R. D. Lewis, O. F. Brandenburg, K. Chen, F. H. Arnold, *ACS Cent. Sci.* **2018**, *4*, 372–377.
- [45] D. Nam, A. Tinoco, Z. Shen, R. D. Adukure, G. Sreenilayam, S. D. Khare, R. Fasan, *J. Am. Chem. Soc.* **2022**, *144*, 2590–2602.
- [46] H. A. Dailey, A. N. Septy, L. Daugherty, D. Thames, S. Gerdes, E. V. Stabb, A. K. Dunn, T. A. Dailey, J. D. Phillips, *mBio* **2011**, *2*, e00248–00211.
- [47] X. Liu, Z. Yuan, J. Wang, Y. Cui, S. Liu, Y. Ma, L. Gu, S. Xu, *Biochem. Biophys. Res. Commun.* **2017**, *484*, 40–44.
- [48] V. Pfanzagl, K. Nys, M. Bellei, H. Michlits, G. Mlynek, G. Battistuzzi, K. Djinovic-Carugo, S. Van Doorslaer, P. G. Furtmüller, S. Hofbauer, *J. Biol. Chem.* **2018**, *293*, 14823–14838.
- [49] M. J. Weissenborn, S. A. Löw, N. Borlinghaus, M. Kuhn, S. Kummer, F. Rami, B. Plietker, B. Hauer, *ChemCatChem* **2016**, *8*, 1636–1640.
- [50] G. Sreenilayam, R. Fasan, *Chem. Commun.* **2015**, *51*, 1532–1534.
- [51] V. Steck, G. Sreenilayam, R. Fasan, *Synlett* **2020**, *31*, 224–229.
- [52] R. D. Lewis, M. Garcia-Borràs, M. J. Chalkley, A. R. Buller, K. Houk, S. J. Kan, F. H. Arnold, *Proc. Natl. Acad. Sci. USA* **2018**, *115*, 7308–7313.
- [53] E. J. Moore, V. Steck, P. Bajaj, R. Fasan, *J. Org. Chem.* **2018**, *83*, 7480–7490.
- [54] M. Garcia-Borràs, S. J. Kan, R. D. Lewis, A. Tang, G. Jimenez-Osés, F. H. Arnold, K. N. Houk, *J. Am. Chem. Soc.* **2021**, *143*, 7114–7123.
- [55] G. Sreenilayam, E. J. Moore, V. Steck, R. Fasan, *Adv. Synth. Catal.* **2017**, *359*, 2076–2089.
- [56] R. Balhara, R. Chatterjee, G. Jindal, *Phys. Chem. Chem. Phys.* **2021**, *23*, 9500–9511.
- [57] A. Tinoco, Y. Wei, J.-P. Bacik, D. M. Carminati, E. J. Moore, N. Ando, Y. Zhang, R. Fasan, *ACS Catal.* **2018**, *9*, 1514–1524.
- [58] R. L. Khade, A. L. Chandgude, R. Fasan, Y. Zhang, *ChemCatChem* **2019**, *11*, 3101.
- [59] D. Kruschel, B. Zagrovic, *Mol. BioSyst.* **2009**, *5*, 1606–1616.
- [60] Q. Cui, M. Karplus, *Protein Sci.* **2008**, *17*, 1295–1307.
- [61] G. G. Dodson, D. P. Lane, C. S. Verma, *EMBO Rep.* **2008**, *9*, 144–150.
- [62] H. Su, G. Ma, Y. Liu, *Inorg. Chem.* **2018**, *57*, 11738–11745.
- [63] R. Ahlrichs, M. Bär, M. Häser, H. Horn, C. Kölmel, *Chem. Phys. Lett.* **1989**, *162*, 165–169.
- [64] W. Smith, T. Forester, *J. Mol. Graphics* **1996**, *14*, 136–141.
- [65] P. Sherwood, A. H. de Vries, M. F. Guest, G. Schreckenbach, C. R. A. Catlow, S. A. French, A. A. Sokol, S. T. Bromley, W. Thiel, A. J. Turner, *J. Mol. Struct.* **2003**, *632*, 1–28.
- [66] D. A. Sharon, D. Mallick, B. Wang, S. Shaik, *J. Am. Chem. Soc.* **2016**, *138*, 9597–9610.
- [67] X. Li, L. Dong, Y. Liu, *Inorg. Chem.* **2020**, *59*, 1622–1632.
- [68] X. Ren, R. Fasan, *Curr. Opin. Green Sustain. Chem.* **2021**, *31*, 100494.
- [69] K. Oohora, A. Onoda, T. Hayashi, *Acc. Chem. Res.* **2019**, *52*, 945–954.
- [70] R. L. Khade, Y. Zhang, *J. Am. Chem. Soc.* **2015**, *137*, 7560–7563.
- [71] H. M. Key, P. Dydio, D. S. Clark, J. F. Hartwig, *Nature* **2016**, *534*, 534–537.
- [72] GaussView, Version 6, R. Dennington, T. A. Keith, J. M. Millam, *Semichem Inc., Shawnee Mission, KS, USA* **2016**.
- [73] M. H. Olsson, C. R. Søndergaard, M. Rostkowski, J. H. Jensen, *J. Chem. Theory Comput.* **2011**, *7*, 525–537.
- [74] P. Li, K. M. Merz Jr, *J. Chem. Inf. Model.* **2016**, *56*, 599–604.
- [75] J. M. Seminario, *Int. J. Quantum Chem.* **1996**, *60*, 1271–1277.
- [76] J. Wang, W. Wang, P. A. Kollman, D. A. Case, *J. Mol. Graphics Modell.* **2006**, *25*, 247–260.
- [77] W. L. Jorgensen, J. Chandrasekhar, J. D. Madura, R. W. Impey, M. L. Klein, *J. Chem. Phys.* **1983**, *79*, 926–935.
- [78] S. O. Waheed, S. S. Chaturvedi, T. G. Karabancheva-Christova, C. Z. Christov, *ACS Catal.* **2021**, *11*, 3877–3890.
- [79] C. Christov, R. Ramanan, S. O. Waheed, C. J. Schofield, *Chem. Eur. J.* **2021**, *27*, 11827–11836.
- [80] R. L. Davidchack, T. Ouldrige, M. Tretyakov, *J. Chem. Phys.* **2015**, *142*, 144114.
- [81] D. K. Chakravorty, B. Wang, C. W. Lee, A. J. Guerra, D. P. Giedroc, K. M. Merz, *J. Biomol. NMR* **2013**, *56*, 125–137.
- [82] F. Bresme, *J. Chem. Phys.* **2001**, *115*, 7564–7574.
- [83] J.-P. Ryckaert, G. Ciccotti, H. J. Berendsen, *J. Comput. Phys.* **1977**, *23*, 327–341.
- [84] A. W. Gotz, M. J. Williamson, D. Xu, D. Poole, S. Le Grand, R. C. Walker, *J. Chem. Theory Comput.* **2012**, *8*, 1542–1555.
- [85] J. A. Maier, C. Martinez, K. Kasavajhala, L. Wickstrom, K. E. Hauser, C. Simmerling, *J. Chem. Theory Comput.* **2015**, *11*, 3696–3713.
- [86] D. R. Roe, T. E. Cheatham III, *J. Chem. Theory Comput.* **2013**, *9*, 3084–3095.
- [87] E. Casali, E. Gallo, L. Toma, *Inorg. Chem.* **2020**, *59*, 11329–11336.
- [88] J. Kästner, J. M. Carr, T. W. Keal, W. Thiel, A. Wander, P. Sherwood, *J. Phys. Chem. A* **2009**, *113*, 11856–11865.
- [89] S. R. Billeter, A. J. Turner, W. Thiel, *Phys. Chem. Chem. Phys.* **2000**, *2*, 2177–2186.

Manuscript received: May 12, 2022

Accepted manuscript online: August 10, 2022

Version of record online: September 23, 2022